Kasetsart J. (Nat. Sci.) 43 : 333 - 339 (2009)

Geometric Study of Relativistic Heavy Ion Collisions

Roppon Picha

ABSTRACT

This study discusses aspects regarding the geometry of high-energy heavy ion collisions in particle accelerators, from which a myriad of new particles are produced. Calculations of the number of participating nucleons and the number of collisions were made, using experimental parameters from existing literature. Three symmetric systems were investigated: copper (Cu-63), gold (Au-197) and lead (Pb-208), which are some of the main elements studied in the Relativistic Heavy Ion Collider (RHIC) and the Large Hadron Collider (LHC) particle accelerators. The calculations showed that as the energy of collision increased from RHIC to LHC energies, the number of collisions approximately doubled, largely due to the increased inelastic cross section.

Key words: special relativity, nuclear, heavy ions, particles, geometry

INTRODUCTION

Strong force

The only way to probe nuclear forces is to have reactions occur at very small-scale distances and at high energy. Collisions between two high-energy projectiles (subatomic particles or atomic ions) can create high energy densities, which will then give rise to a myriad of new particles. While only protons, neutrons and electrons are stable entities, short-lifetime particles such as pions, kaons and lambdas can be produced copiously and their existences can be evidenced via their decay channels. Weak nuclear forces can be observed as beta decays of radioisotopes. Strong nuclear force is modeled as the attractive force that keeps the nucleons together inside the nucleus and causes the confinement of quarks. The physics of confinement is not well understood and its theoretical formulation was the subject of the 2004 Nobel Prize in Physics (Gross and Wilczek, 1973; Politzer, 1973).

High energy collisions

The studies of heavy ion collisions at relativistic energies have yielded interesting results in different regions of transverse momentum. In the low momentum region, collective expansion is evidenced in anisotropic flow (Ollitrault, 1998). Jet suppression has also been observed at high momentum (Adams, 2004), which has been interpreted as partons losing energy in the dense, colored, medium of deconfined quarks and gluons.

At high temperature, normal matter can turn from the gas phase to a plasma phase, in which atoms are ionized. Due to Coulomb repulsion, a great amount of energy is required to cause the two like-charge particles to fuse. Under extreme conditions, protons and neutrons will become a different type of plasma, where the charge is not electric, but colored. This is called quark-gluon plasma (QGP). The strong force between colored quarks is attractive, which quickly brings the quarks back to hadrons. The collision energy is redistributed to create particles different from the

Thailand Institute of Nuclear Technology (TINT), 16 Vibhavadi Rangsit Rd, Chatuchak, Bangkok 10900, Thailand.
E-mail: aeroppon@gmail.com

initial nucleons. Quantum chromodynamics (QCD) has predicted that a phase change from hadronic matter to plasma with free quarks should occur, if the temperature is sufficiently large (Shuryak, 1978; Bjorken, 1983; Karsch, 2002). As the system expands, the temperature will drop, and the parton plasma of quarks and gluons will transform back into hadronic matter (matter made of confined quarks and gluons). The study of relativistic, heavy ion collisions thus provides a unique opportunity to understand QGP right here on Earth.

Collisions between two heavy ions are considered a large system in particle physics experiments, but in reality, they are only at the femtometer scale. In collisions occurring in a Relativistic Heavy Ion Collider (RHIC) and a Large Hadron Collider (LHC), the particles travel near the speed of light and the kinetic energy is described by the special relativity equation, $KE = E–mc^2$. The goal of heavy ion collisions is not so much to study the individual particles themselves, but large-scale evolution; it is not the collision itself that is of prime importance, but rather what happens after the collision.

Phase transition

The phases of hadronic matter are shown in Figure 1. This is analogous to the phase diagram of water. As heat is added or removed, the intermolecular bond energies will change, leading to the loosening or tightening of chemical bonds, and water transforming its phase. For nuclear matter, the hadron gas is expected to break down into plasma of quarks and gluons at some point. Instead of studying temperature and pressure as in normal matter, with hadronic matter, it is usual to calculate temperature and baryon density.

The collisions inside high-energy particle accelerators provide a system where net baryon density is small, but the temperature is extremely high (of the order 100 MeV). This system provides an ideal laboratory for scientists to investigate the properties of QGP. The near-zero baryon density

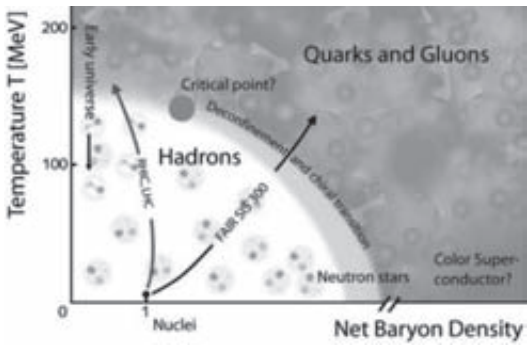

Figure 1 A sketch of a possible phase diagram for hadronic matter. (source: FAIR @ GSI).

closely resembles the proposed state of the early universe, where antimatter and matter existed in equal amounts.

MATERIALS AND METHODS

Size of the nucleus

Stable, heavy nuclei of mass numbers around 200 and radii 7 fm were used. The system of heavy ions is considered large compared to the collisions between elementary particles, such as protons or electrons in other high-energy particle accelerators. However, it is still tens of thousands times smaller than atomic sizes. Comparatively, the human body is about a million times smaller than the Earth. The size of a heavy ion collision is only about 10^{-15} times as large as the human body.

If the nuclear density is uniform throughout (hard sphere model), then the density of the nucleus of mass number A is shown by Equation 1:

$$\frac{A}{V} = \frac{A}{4\pi R^3/3} = \text{constant} \qquad (1)$$

then $R \propto \sqrt[3]{A}$. The proportionality constant in Equation 1 is about 1.2 fm. This yields the radii of Cu-63, Au-197 and Pb-208 as R_{Cu}= 4.77 fm, R_{Au}= 6.98 fm and R_{Pb}= 7.11 fm, respectively.

Let r be a distance from the nuclear center and $\rho(r)$ be the density at that point. In the hard sphere model, for a nucleus of radius R, the number density is $3/(4\pi R^3)$ for $r \leq R$ and zero when $r > R$. The current calculations and Equation 2 treat the nuclear density as a Woods-Saxon profile (Woods and Saxon, 1954):

$$\rho(r) = \frac{\rho_0}{1 + \exp((r - r_0)/a)} \quad (2)$$

where ρ_0 = density at the nuclear center, r_0= mean radius and a = a fit parameter.

Values can be used from experiments (de Jager *et al.*, 1974) of each nuclide species. The density constant ρ_0 is treated as the normalization factor.

It must be noted that r_0, which indicates the radius, will be compressed along the beam direction by the Lorentz factor. Thus, the nucleus will look like an ellipse with a major radius of $2r_0$ and a minor radius of $2r_0/\gamma$ where γ is the relativistic gamma factor.

Geometry of the collision

The geometry of the initial state will affect the final state results. The collisions between large nuclei differ in geometry from the collisions of electrons or even protons. A starting point is to specify the directional axes, with the beam direction as the z-direction. The two orthogonal axes can be called x and y. The maximum energy at RHIC is 100 GeV/nucleon. The relativistic gamma factor is around 108. At LHC, the maximum energy is 2.75 TeV, which yields the gamma factor of 2963. From these values, the velocities can be calculated as 0.999957412 (RHIC) and 0.999999943 (LHC), in the units of c. The gamma factor also indicates the length contraction in the direction of the beam. The dimensions remain the same orthogonal to the beam.

The impact parameter (b) is the distance between the nuclear centers of the colliding projectiles. The vectors $\vec{b}$ and $\vec{z}$ define the reaction plane.

The thickness function is given by Equation 3:

$$T(\vec{s}) = T(s) = \int_{-\infty}^{\infty} \rho(s,z)dz \quad (3)$$

with the normalization condition in Equation 4:

$$\int T(s)\, d^2s = \iint \rho(s,z)\, dz\, d^2s = A \quad (4)$$

The thickness function has the unit of 1/area.

The vectors $\vec{s}$ and $\vec{z}$ define the reaction plane, where $\vec{s}$ is normal to the beam direction ($\vec{z}$). Although the nucleus appears squeezed in the beam axis due to relativistic contraction, the integral in the thickness function will be over the full range. Thus, the thickness function is independent of the Lorentz factor.

The overlap function is defined in Equation 5:

$$T_{AB}(b) = \int T_A(s) \cdot T_B(|\vec{b} - \vec{s}\,|)\, d^2s \quad (5)$$

The normalization condition is defined by Equation 6:

$$\int T_{AB}(b)\, d^2b = AB \quad (6)$$

where, A and B are the mass numbers.

Table 1 Parameters used in Woods-Saxon nuclear density function.

Nuclide	r_0 (fm)	a (fm)	ρ_0 (fm^{-3})
Cu-63	4.21	0.586	0.1701
Au-197	6.38	0.535	0.1693
Pb-208	6.62	0.549	0.1600

RESULTS

Cross sections

The probability of interaction between each pair of nucleons (of atomic numbers Z_1 and Z_2; neutron numbers N_1 and N_2; and mass numbers A_1 and A_2) depends on the cross sections of the pair (proton-proton: σ_{pp}, neutron-neutron : σ_{nn}, and proton-neutron: σ_{pn}). The general expression for the nucleon-nucleon cross section can be written as Equation 7:

$$\sigma_{NN} = \frac{\sigma_{pp} Z_1 Z_2 + \sigma_{nn} N_1 N_2 + \sigma_{pn}(Z_1 N_2 + Z_2 N_1)}{A_1 A_2} \quad (7)$$

In general, the neutron data is incomplete over a large energy range. Thus, the proton-proton cross section can be used to represent the nucleon-nucleon data. This is possible because the cross sections are similar. (Under the theory of strong interactions, neutrons and protons are two states of the same particle; they have isospin symmetry.) The closeness of values is shown in Figure 2. For the proton-proton cross sections, the values tabulated in Amsler *et al*. (2008) were used to compare the cross sections at $\sqrt{s_{NN}}$ (center-of-mass energy) of 20, 63, 200, and 5500 GeV by kinematical analysis.

Incident momentum

The Mandelstam variable,*s*, is related to the collision energy as shown in Equation 8:

$$s = (p_1 + p_2)^2 = (E_1 + E_2)^2 - (\vec{p}_1 + \vec{p}_2)^2 = m_1^2 + m_2^2 + 2E_1E_2 - 2\vec{p}_1 \cdot \vec{p}_2 \quad (8)$$

where, p_1 and p_2 are four-momenta, $E_1$and E_2 are energy, $\vec{p}_1$ and $\vec{p}_2$ are three-momenta, and m_1 and m_2 are masses.

The incident momentum in the fixed-target reference frame can be calculated next. Using the invariance of four-momentum scalar products, the momentum of the incident particle can be expressed as Equation 9:

$$|\vec{p}'_{1x}| = \sqrt{\frac{\left[(E_1 + E_2)^2 - (m_1 + m_2)^2\right]^2 - 4m_1^2 m_2^2}{4m_2^2}} \quad (9)$$

For the symmetric case, $E_1 = E_2$ and $m_1 = m_2$, which leads to Equation 10:

$$|\vec{p}'_{1x}| = \frac{2E}{m}\sqrt{E^2 - m^2} \quad (10)$$

The values are listed in Table 2.

From values in Amsler *et al*. (2008), it can be observed that the elastic cross section stabilizes at around 7.6 ± 0.3 mb for the momentum beyond 1 TeV/c. The inelastic values, in contrast, increase with the momentum. The inelastic cross

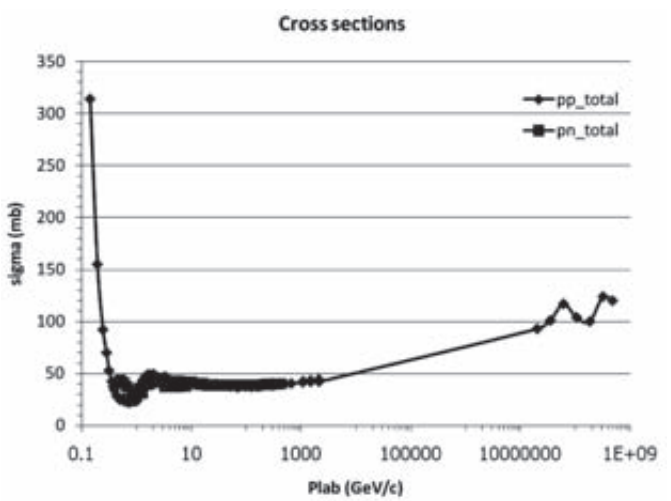

Figure 2 The total cross sections for proton-proton compared to proton-neutron.

Table 2 Corresponding momentum at each collision energy.

E_{beam} (GeV/nucleon)	p (GeV/c)
10	213.7
31.2	2,089.1
100	21,469.8
2750	16,237,250.8

sections can now be interpolated. In the momentum range of 10-100 GeV/c, the total cross section σ_{tot} does not change much, remaining at around 39-44 mb, but it will jump at momentum $1.6x10^7$ GeV/c to about 90±14 mb. The values of the cross section at extremely high energies have been measured in air shower experiments at the Akeno Cosmic Ray Observatory (Honda *et al.*, 1993).

The total cross sections are taken to be σ_{tot} = 39 ± 1 mb at 20 GeV, σ_{tot} = 44.0 ± 0.4 at 62.4 GeV, σ_{tot} = 42.2 ± 3.5 mb at 200 GeV, and σ_{tot} = 90 ± 14 mb at 5.5 TeV. The elastic cross sections are σ_{el} = 6.9 ± 0.5 mb at 20 GeV and σ_{el} = 7.6 ± 0.3 mb at 62.4 GeV, 200 GeV, and 5.5 TeV. Thus, the inelastic cross sections can be estimated as: σ_{20GeV} = 32.1 ± 1.1 mb, $\sigma_{62.4GeV}$ = 36.4 ± 0.5 mb, σ_{200GeV} = 34.6 ± 3.5 mb and $\sigma_{5.5TeV}$ = 82.4 ± 14.0 mb.

Collision probability

The probability of a collision (a hit) at impact parameter *b* is given by Equation 11:

$$P(b) = \frac{N_{\text{coll}}(b)}{N_{\text{coll,max}}} = \frac{\sigma_{pp} \cdot T_{AB}(b)}{AB} \qquad (11)$$

where, $N_{coll}(b)$ is the number of collisions at *b* and $N_{coll,max}$ is the maximum number of collisions.

The probability of getting *n* collisions at *b* is (Equation 12):

$$P_{AB}(n,b) = \binom{AB}{n}\left(\frac{\sigma_{pp} \cdot T_{AB}(b)}{AB}\right)^n\left(1-\frac{\sigma_{pp} \cdot T_{AB}(b)}{AB}\right)^{AB-n}$$

$$= \binom{AB}{n}\left(\frac{N_{coll}(b)}{AB}\right)^n\left(1-\frac{N_{coll}(b)}{AB}\right)^{AB-n} \qquad (12)$$

From the binomial expansion, this can be written in Equation 13 as:

$$\sum_{n=1}^{AB} P_{AB}(n,b) = \sum_{n=1}^{AB}\binom{AB}{n}\left(\frac{N_{coll}(b)}{AB}\right)^n\left(1-\frac{N_{coll}(b)}{AB}\right)^{AB-n}$$

$$= \left[\frac{N_{coll}(b)}{AB}+1-\frac{N_{coll}(b)}{AB}\right]^{AB} - \left[1-\frac{N_{coll}(b)}{AB}\right]^{AB}$$

$$= 1-\left[1-\left(\frac{N_{coll}(b)}{AB}\right)\right]^{AB} \qquad (13)$$

where, $\binom{a}{b} = \frac{a!}{b!(a-b)!}$..

To simplify the expression, the approximation in Equation 14 can be applied:

$$\left[1-\frac{\sigma_{pp} \cdot T_{AB}(b)}{AB}\right]^{AB} \cong \exp(-\sigma_{pp} \cdot T_{AB}(b))$$

$$= \exp(1-N_{coll}(b)) \qquad (14)$$

Participating nucleons and number of collisions

The number of participating nucleons (participants, N_{par}) can be calculated from thickness functions as (Equation 15):

$$N_{par}(b) = \int [T_A(s)\cdot(1-\exp(-\sigma_{inel}T_B(|\vec{b}-\vec{s}|))) + T_B(|\vec{b}-\vec{s}|)\cdot(1-\exp(-\sigma_{inel}T_A(s)))]d^2s \qquad (15)$$

The graph in Figure 3 shows the number of participating nucleons between different symmetric systems, with σ_{inel} set at 36 mb. The number of binary collisions will be proportional to the overlap function and the cross section. The number of collisions can be expressed as a function of the impact parameter $N_{coll}(b) = \sigma_{NN}.T_{AB}(b)$. Collision numbers, as functions of b, are graphed in Figure 3.

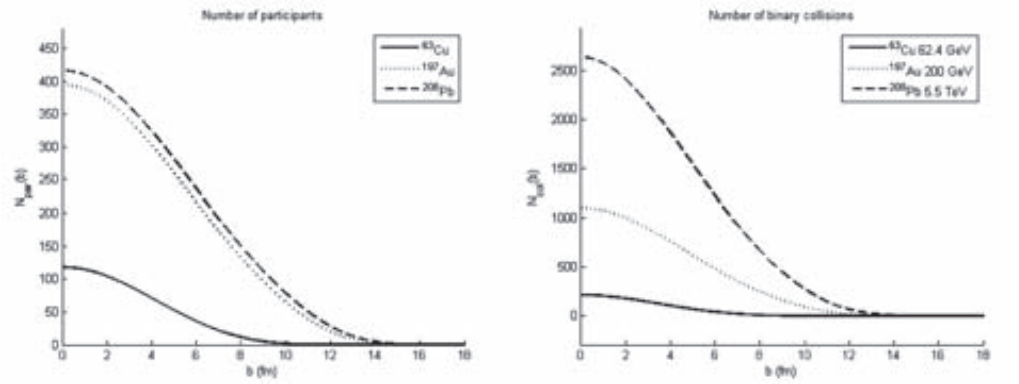

Figure 3 Left: The number of participating nucleons for Cu-63, Au-197 and Pb-208 systems. Right: The number of binary collisions for Cu-63 at S_{NN} = 62.4 GeV, Au-197 at S_{NN} = 200 GeV and Pb-208 at S_{NN} = 5.5 TeV.

DISCUSSION

The cross section of the nucleon-nucleon collisions could be calculated using experimental proton-proton data. The estimated inelastic cross sections (σ_{20GeV} = 32.1 ± 1.1 mb, $\sigma_{62.4GeV}$ = 36.4 ± 0.5 mb, σ_{200GeV} = 34.6 ± 3.5 mb and $\sigma_{5.5TeV}$ = 82.4 ± 14.0 mb, obtained via interpolation) showed a significant increase with the collision energy.

The probability of getting *n* collisions at *b* was obtained by taking the combination of both, which was expanded into a binomial form.

The results showed that the number of participating nucleons did not change substantially between the Au-Au system and the Pb-Pb system. The inelastic cross sections had larger effects when the number of binary collisions was calculated. It can be concluded that the maximum number of participating nucleons in Pb-208 collisions increased by more than twofold of that in Cu-63 collisions. In peripheral collisions, both the number of participants and the number of collisions appeared to fall to the minimum value (zero) for all the systems when the impact parameter was above 13 fm.

CONCLUSIONS

Kinematic and geometric analyses of the heavy ion collisions in the relativistic regime of RHIC and LHC were studied. In a collision between two large nuclei, the production of particles depended on the impact parameter of the collision and the inelastic cross section. The gold and lead ions yielded similar density profiles, as well as similar numbers of participating nucleons. The higher energy at the LHC, however, increased the inelastic cross section to be about twice as large, resulting in a higher number of collisions that should produce a more dense initial state. The collective effects found at RHIC should remain visible at LHC.

LITERATURE CITED

Adams, J. *et al*. 2004. Azimuthal anisotropy and correlations at large transverse momenta in p+p and Au+Au collisions at sNN=200 GeV. **Phys. Rev. Lett**. 93: 252301-252306.

Amsler, C. *et al*. 2008. The 2008 review of particle physics. **Phys. Lett. B** 667(1).

Bjorken, J. D. 1983. Highly relativistic nucleus-nucleus collisions: The central rapidity region. **Phys. Rev. D** 27: 140-151.

de Jager, C. W., H. de Vries and C. de Vries. 1974. Nuclear charge- and magnetization-density-distribution parameters from elastic electron scattering. **At. Data Nucl. Data Tables** 14: 479-508.

Gross, D. J. and F. Wilczek. 1973. Asymptotically free gauge theories. I. **Phys. Rev. D** 8: 3633-3652.

Honda, M., M. Nagano, S. Tonwar, K. Kasahara, T. Hara, N. Hayashida, Y. Matsubara, M. Teshima and S. Yoshida. 1993. Inelastic cross section for p-air collisions from air shower experiments and total cross section for p-p collisions up to sqrt(s) =24 TeV. **Phys. Rev. Lett**. 70: 525-528.

Karsch, F. 2002. Lattice results on QCD thermodynamics. **Nucl. Phys. A** 698: 199-208.

Ollitrault, J. Y. 1998. Flow systematics from SIS to SPS energies. **Nucl. Phys. A** 638: 195-206.

Politzer, H. D. 1973. Reliable perturbative results for strong interactions. **Phys. Rev. Lett.** 30: 1346-1349.

Shuryak, E. V. 1978. Quark-gluon plasma and hadronic production of leptons, photons and psions. **Phys. Lett. B** 78: 150-153.

Woods, R. D. and D. S. Saxon. 1954. Diffuse surface optical model for nucleon-nuclei scattering. **Phys. Rev.** 95: 577-578.